



Published in final edited form as:

Clin Cancer Res. 2016 June 1; 22(11): 2668–2674. doi:10.1158/1078-0432.CCR-15-2429.

Voxel level radiologic-pathologic validation of Restriction Spectrum Imaging cellularity index with Gleason grade in Prostate Cancer

Ghiam Yamin^{1,†}, Natalie M. Schenker-Ahmed^{1,†}, Ahmed Shabaik², Dennis Adams², Hauke Bartsch¹, Joshua Kuperman¹, Nathan S. White¹, Rebecca A. Rakow-Penner¹, Kevin McCammack¹, J. Kellogg Parsons³, Christopher J. Kane³, Anders M. Dale^{1,4}, and David S. Karow¹

¹Department of Radiology, University of California San Diego School of Medicine, San Diego, CA, USA

²Department of Pathology, University of California San Diego School of Medicine, San Diego, CA, USA

³Department of Surgery, University of California San Diego School of Medicine, San Diego, CA, USA

⁴Department of Neurosciences, University of California, San Diego, La Jolla, CA, USA

Abstract

Purpose—Restriction spectrum imaging (RSI-MRI), an advanced diffusion imaging technique, can potentially circumvent current limitations in tumor conspicuity, *in-vivo* characterization, and location demonstrated by multiparametric magnetic resonance imaging (MP-MRI) techniques in prostate cancer (PCa) detection. Prior reports show that the quantitative signal derived from RSI-MRI, the cellularity index, is associated with aggressive PCa as measured by Gleason grade (GG). We evaluated the reliability of RSI-MRI to predict variance with GG at the voxel-level within clinically demarcated PCa regions.

Experimental Design—Ten cases were processed using whole mount sectioning after radical prostatectomy. Regions of tumor were identified by a uropathologist. Stained prostate sections were scanned at high resolution (75 μ m/pixel). A grid of tiles corresponding to voxel dimensions was graded using the GG system. RSI-MRI cellularity index was calculated from presurgical prostate MR scans and presented as normalized z-score maps. In total, 2,795 tiles were analyzed and compared with RSI-MRI cellularity.

Results—RSI-MRI cellularity index was found to distinguish between PCa and benign tumor ($t=25.48$, $p<0.00001$). Significant differences were also found between benign tissue and PCa classified as low-grade (GG=3; $t=11.56$, $p<0.001$) or high-grade (GG 4 $t=24.03$, $p<0.001$). Furthermore, RSI-MRI differentiated between low and high-grade PCa ($t=3.23$, $p=0.003$).

Corresponding author: David S Karow.

[†]These authors contributed equally to this work.

Authors declare no conflict of interests

Conclusions—Building on our previous findings of correlation between GG and the RSI-MRI among whole tumors, our current study reveals a similar correlation at voxel resolution within tumors. Because it can detect variations in tumor grade with voxel-level precision, RSI-MRI may become an option for planning targeted procedures where identifying the area with the most aggressive disease is important.

Keywords

RSI-MRI; prostate cancer; Gleason grade; diffusion-weighted imaging; digital pathology

Introduction

Prostate cancer (PCa) is the most common non-cutaneous cancer and the second leading cause of cancer death in U.S. men [1]. Most prostate cancers are adenocarcinomas (95%) that develop from prostatic gland secretory luminal cells; ~70% arise in the peripheral zone [2,3], ~20-25% arise in the transition zone [3,4], and ~8% arise in the central zone [3]. Randomized trials have confirmed the efficacy of prostate-specific antigen (PSA) population screening to diminish prostate cancer mortality. [5]. However, aggressive population screening with PSA increases the detection of both lethal and non-lethal cancers, which can promote over-detection and over-treatment of non-lethal cancers. Decreasing prostate cancer mortality while minimizing the potential morbidities of over-detection and over-treatment requires refined approaches to screening and diagnosis using novel, non-invasive biomarkers to differentiate indolent from clinically significant disease.

Multiparametric magnetic resonance imaging (MP-MRI) is a rapidly evolving non-invasive diagnostic tool that has been used to complement other emerging biomarkers in the screening, staging, monitoring, and treatment of PCa [6]. However, prostate MRI is confounded by variable sensitivity (36-100%) and specificity (64-95%), which curtails its clinical utility [7,8]. Diffusion weighted imaging (DWI), an advanced MRI modality, detects the impeded diffusivity of water in the intra- and extracellular compartments and has shown correlation with PCa. However, DWI is limited by magnetic field inhomogeneity and high false positive rates from inflammation, hemorrhage, or benign nodules in the transitional zone, which limit tumor conspicuity and location [9].

Restriction spectrum imaging (RSI-MRI) is an advanced imaging technique that shows improved conspicuity and differentiation of solid tumors compared to traditional diffusion weighted imaging methods [10,11]. The RSI-MRI method can differentiate hindered vs. restricted diffusion, thought to correspond to the extracellular and intracellular water compartments, respectively [12]. RSI-MRI demonstrates improved signal-to-noise in tumor detection and exhibits reduced spatial distortion. We previously reported that the RSI-MRI cellularity index is associated with the detection of aggressive PCa as defined by Gleason grade [13], and RSI-MRI provides improved sensitivity in the detection of extraprostatic extension of PCa compared to standard MRI [14]. In order to account for tumor grade heterogeneity within and between tumors, we sought to analyze histopathological whole mount (WM) PCa section at the voxel level. We hypothesized that pathology grading at this level of resolution would provide a more accurate representation of the intra-tumor

variability that may be masked within an overall grade assigned to large tumor regions of interest (ROIs). Here, we report the correlation of voxel-level Gleason graded PCa specimens with RSI-MRI and discuss possible diagnostic and prognostic information gained from such analyses.

Materials and Methods

Restriction Spectrum Imaging

All patients in this institutional review board approved study were previously diagnosed with PCa status post ultrasound-guided transrectal biopsy. Prior to radical prostatectomy, a pelvic MRI was performed to aid in surgical planning. Patients were scanned using a 3.0-T Signa HDxt MRI Scanner (General Electric) and a cardiac coil; no endorectal coil was used. The entire prostate was imaged, with axial slices oriented perpendicular to the rectal wall. T2-weighted images were acquired using a fast spin echo protocol with 3.0 mm contiguous slices. The RSI-MRI protocol parameters included b -values of 0, 125 (6 unique directions), 375 (6 unique directions), and 1000 (15 unique directions) s/mm^2 . The RSI-MRI protocol increased the total duration of the MRI scan time by five minutes. Additional details of the pulse sequence parameters can be found in Supplementary Table 1. RSI-MRI maps were reconstructed based on all b -values and standardized across the sample to produce the z -score cellularity map. Specifically, z -score cellularity maps were produced using mean and standard deviations of normal prostate signal from the raw RSI-MRI maps in the benign tissue in the patient population, subtracting the mean value from an individual subjects' RSI-MRI cellularity map, and dividing by the benign prostate standard deviation. Corrections for spatial distortion due magnetic field inhomogeneity in echo planar imaging were accomplished with an alternating phase-encode technique [15]. After correction for spatial distortion, RSI-MRI maps were co-registered to the T2 images.

Digital histopathology & scoring

In general, the radical prostatectomy cases were consecutive surgeries, however some cases were excluded because of significant artifacts in the histology, which would have made co-registration nearly impossible. Status-post radical prostatectomy, WM histopathology was performed on 5- μ m thick sections. Each hematoxylin and eosin (H&E) stained histopathological section was reviewed by a board-certified surgical pathologist (AS), who demarcated ROIs corresponding to tumor. The H&E digital images were acquired with a Keyence BZ-X710 All-in-one fluorescence microscope (Osaka, Japan) using transmitted light with a CFI Plan Apo λ 10x objective lens. To image the entire tissue section, the perimeter of the stained tissue was marked using low magnification (2X), and then automatically acquired with the 10X objective. The microscope automatically focused each image tile of the mosaic. Exposure time and white balance were calculated automatically by the system. All scans were acquired at high resolution (0.75488 μ m/pixel). Tiles representing the entire image were then reconstructed into a "digital prostate map" interface and tumor ROIs overlaid with an alphanumeric grid containing tiles corresponding to voxel dimensions as shown in (Figures 1 and 2).

Gleason grade is the gold standard for grading prostate cancer aggressiveness [16–18], and is used to categorize prostate tissue based on histological patterns. Tissue is given a grade from 1–5, with larger numbers typically indicating more aggressive cancer, characterized by poorly differentiated tissue, and, generally, a worse prognosis. Each tile in the overlaid alphanumeric grid was assessed for primary Gleason grade. Scoring for the current study focused on the primary grade that covered greater than 51% of the tile area, despite presence of other secondary grades that were higher or lower. For example, if 60% of the tile represented GG 4 but the rest was GG 5 (traditionally assigned a 4 + 5 Gleason score pattern), the final GG used for that tile in this study would be GG 4. Following current practice, only tiles with tissue of grades 3–5 were assigned a score; other tiles were scored as benign. A score of 0 was used to represent a benign area. Scored digital tiles were reviewed for accuracy by the same uropathologist who reviewed the H&E stained histopathological slide. A recent similarly conceptualized scoring framework, based on a five-grade group system founded on Gleason score, has shown improved risk stratification compared to the modern Gleason scoring system [17].

Registration of RSI-MRI with histopathology

A radiologist with experience in prostate cancer MR imaging (DSK) selected the slice from the T2 MRI series that corresponded most closely to the plane of the histopathology section. To correct for deformation of the 2D slice that may have occurred during histological processing, the Control Point Selection Tool in MATLAB (Release 2010b, The MathWorks, Inc., Natick, Massachusetts, United States) was used to affine transform the selected T2 MRI slice to the shape and dimension of the histopathology section. The same transformation was applied to the registered RSI-MRI cellularity maps (Figure 2). Anatomical landmarks, including the prostate shape, position of the urethra, and prominent benign prostatic hyperplasia nodules, were used to align the T2 MRI image as much as possible to the whole-mount sections. The Euclidean distance between transformed points and target points was calculated. The average registration error across all ten subjects was 1.84 μm .

Statistical Analysis

Linear mixed-effect with a random effect [19] of subject was used to determine the effectiveness of RSI-MRI in detecting tumor aggressiveness, by comparing benign tissue to increasingly aggressive tissue (benign vs. low grade PCa (Gleason 3) vs. high grade PCa (Gleason 4 and Gleason 5)). Post-hoc multiple comparison *t*-tests [20] were used to assess RSI-MRI's ability to differentiate between normal prostate tissue and different levels of tumor aggressiveness (benign vs. low grade PCa and benign vs. high grade PCa) and between tumor grades (low grade PCa vs. high grade PCa). Statistical significance, *p*-value <0.05, was determined using the software program R [21]. The data then were plotted using SigmaPlot 12.5 (Systat Software Inc., San Jose, CA).

Results

Ten patients, representing a range of tumor aggressiveness, who were evaluated with a preoperative MRI and RSI-MRI underwent radical prostatectomy and underwent surgery

between March 2014 to December 2014 with WM specimens (Table 1). T2-weighted MRI images and RSI-MRI cellularity maps were co-registered with the WM prostate histopathological section as depicted in four cases (Figure 2). The ten WM PCa cases encompassed 17 tumor ROIs. Two patients had two distinct tumor ROIs, one patient had three distinct tumors ROIs, and another patient had four distinct tumor ROIs within one specimen. All patients with 2 ROIs had concordant tumors. Tumor ROIs were overlaid with an alphanumeric grid (Figure 1), with the size of each square of the grid corresponding to the voxel dimensions used for acquisition of the RSI-MRI. We analyzed 2,795 total squares of WM prostate H&E-stained sections, of which 1,573 and 1,222 (Gleason 3: 267; Gleason 4: 392; Gleason 5: 563) comprised benign and tumor tissue, respectively.

RSI-MRI data for both normal and tumor regions were normally distributed. The mean cellularity index in PCa was 1.81 (S.E.M.=0.05) and in benign tissue was -0.32 (S.E.M.=0.03). A linear mixed-effect with a random effect [19] of subject was employed to determine the association of RSI-MRI cellularity index with PCa (benign vs. low grade PCa vs. high grade PCa) (Table 2). RSI-MRI cellularity index distinguished benign from increasingly malignant PCa ($p < 1 \times 10^{-5}$) (Table 2). Both low- and high-grade PCa showed significant differences in RSI-MRI signal compared to benign tissue (both $p < 0.001$) (Table 3). Furthermore, significant difference in the RSI-MRI signal between pathological categories, namely between low- and high-grade PCa, was observed ($p = 0.003$) (Table 3). Of note, we observed a trend of higher mean RSI-MRI cellularity with increasing grade (Gleason 3 through Gleason 5) versus benign tissue (Figure 3). By leaving out either individual voxels or individual subjects, we conducted leave-one-out analyses, and in each case recalculated the model and predicted the left out RSI-MRI values using the new model. The resulting root mean squared errors from this analysis were 1.425 and 1.618 for leaving out voxels and subjects, respectively.

Discussion

We analyzed voxel-level Gleason-graded histopathological samples in comparison with RSI-MRI cellularity indices obtained from pre-surgical *in-vivo* MR scans. The data from the current study build on our previous findings of correlation between Gleason grade and the RSI-MRI cellularity index at the tumor level in a sample that included the ten patients in the current study [22] and reveal a correlation between the same parameters at the voxel-level, demonstrating the ability of the RSI-MRI cellularity index to detect variation of Gleason grade within a single tumor.

MP-MRI is currently regarded as the standard of care noninvasive imaging biomarker for diagnosing and staging prostate cancer, despite its variable reliability in providing accurate diagnosis. The RSI-MRI method overcomes the limitations of DWI in MP-MRI by minimizing the extracellular diffusivity (or hindered component) seen in conventional DWI and capitalizing on the intracellular signal diffusivity (or restricted component) to detect regions of high cellularity, which can be associated with increased tumor burden [13,14]. RSI-MRI presents several advancements to currently implemented MP-MRI tumor imaging, including improved signal-to-noise in tumor detection and reduced spatial distortion.

RSI-MRI is designed to optimize the signal from the restricted intracellular water compartment, which is increased in tumor cells [12]. Although Gleason grade is not a direct measure of cellularity, it is qualitatively based on architectural features that may indirectly relate to cellularity. Therefore, we expect the RSI-MRI cellularity index to correlate with tumor aggressiveness as measured by pathological grade or Gleason grade. Novel to the traditional method of Gleason reporting and its application to radiologic-pathologic correlation with RSI-MRI, is our use of WM histopathological sections scored at the voxel level. Traditionally, the pathologist highlights a tumor ROI and reports a general score for that area. In fact, this methodological approach was used recently to demonstrate that RSI-MRI detects increasingly aggressive PCa, as defined by Gleason scores [13]. We performed voxel-level pathological grading with the rationale that pathological assessment at this level of resolution is a more accurate representation of tumor variability. It is possible that the heterogeneity of different tumor grades may be masked within an overall grade assigned to large tumor ROIs.

Our previous studies [13,22] have demonstrated the ability of RSI-MRI to discriminate among different grades of prostate cancer on a tumor-by-tumor basis. This study takes those findings to a resolution that is at least two orders of magnitude higher. Instead of analyzing each tumor as a whole, we analyzed each tumor at the level of the RSI-MRI voxel resulting in hundreds of samples per subject. This enabled us to investigate the ability of RSI-MRI to detect pathological variation within tumors. In concordance with our prior radiologic-pathologic correlation performed on ROIs [13], the data in the current study demonstrate that the RSI-MRI cellularity index distinguishes between PCa aggressiveness within tumors' Gleason grade at the voxel level.

The ability of RSI-MRI to differentiate tumor aggressiveness (low-grade vs. high grade) could have clinical implications in regards to PCa management and treatment. Patients with low-grade disease are candidates for active surveillance. In contrast, patients with high-grade disease are subject to more aggressive treatment (radiation, surgery, and/or hormonal therapy) [6]. The goal of active surveillance is to detect aggressive forms of PCa that have metastatic potential while actively monitoring indolent tumors. Knowledge of pathologic progression during monitoring, aided by a non-invasive method, could improve our management decisions in determining treatment. In this regard, serial imaging with RSI-MRI may afford the clinician an opportunity to monitor disease progression and assist in determining when biopsy is necessary. Furthermore, the ability of RSI-MRI to detect within tumor variability has implications for targeted treatments or procedures, such as MRI guided fusion biopsies. With this novel technology, such biopsies would be better able to target the foci that contain the highest grade of disease. Similarly, evolving image guided focal therapies could conceivably target the area of the highest grade disease with voxel-level precision.

Limitations of our study include restricted patient sample pool (ten patients). However, this is mitigated by large sample size (>2,700) based on our voxel-based analysis, which is a novel approach that is not previously reported elsewhere. Other possible limitations include potential signal co-registration artifacts by tumor burden adjacent to the prostate boundary. Further limitations include lack of secondary pathological characteristic by not accounting

for areas of primary score vs. secondary score. Truly heterogeneous tumors that exhibit intermixing of different Gleason grades can confound simple grading criteria, especially if tumor characteristics represent a hybrid of 2 different grades. We contend that secondary pathologic characteristics are less likely when examining the histopathology at voxel-level accuracy versus whole tumors.

Moreover, because Gleason grade does not directly represent cellularity, it may not be the most effective measure for understanding how RSI-MRI reflects tissue components. For instance, we expect that RSI-MRI will have lesser ability to detect low-grade disease (GG 3), however, in certain cases (e.g. Figure 2, Case 2), we find that the RSI-MRI signal is greater within the tumor than we would expect. In such cases, quantitative analysis of tissue compartments, such as the glandular structure and cell number and density, may yield a greater understanding of the nature of the RSI-MRI signal. Future studies are planned to determine the relationship of RSI-MRI to quantitative tumor cellular characteristics, including extracellular, intracellular, and intranuclear compartments.

Another interesting question not addressed in this study is the issue of variation between different zones within the prostate that is apparent in both MRI and in histology. [23,24] We have not yet investigated the variability of RSI-MRI signal among tumors in different regions. Future studies investigating this issue will require more cases with tumor burden in a wide variety of locations in order to answer this question.

Conclusions

Building on our previous findings of correlation between GG and the RSI-MRI among whole tumors, our current study reveals a similar correlation at voxel resolution within tumors. The relationship between GG and RSI-MRI suggests that RSI-MRI may be used as a component of active surveillance to non-invasively detect high-grade cancer and affect staging and treatment. Furthermore, because it can detect variations in tumor grade with voxel-level precision, RSI-MRI may be a promising option for planning of focal procedures, such as MRI guided targeted biopsies and targeted radiotherapy, where identifying the area with the most aggressive disease is particularly important.

Supplementary Material

Refer to Web version on PubMed Central for supplementary material.

Acknowledgments

Financial Support: This work was supported by the Department of Defense (DoD) Grant, Prostate Cancer Research Program (#W81XWH-13-1-0391), the American Cancer Society—Institutional Research Grant (#70-002), UCSD Clinician Scientist Program (#5T32EB005970-07), UCSD School of Medicine Microscopy Core, and NINDS P30 core grant (#NS047101), and General Electric, Investigator Initiated Research Award BOK92325. This material is based upon work supported by the National Science Foundation under Grant No. 1430082.

References

1. American Cancer Society. Cancer Facts & Figures 2015. Atlanta; 2015.

2. Epstein, JI. The Lower Urinary Tract and Male Genital System. In: Jumar, V.; Abbas, AK.; Fausto, N., editors. Robbins Cotran Pathol Basis Dis. 7th. Philadelphia, PA: Saunders; 2004. p. 1050-8.
3. McNeal JE, Redwine Ea, Freiha FS, Stamey Ta. Zonal Distribution of Prostatic Adenocarcinoma: Correlation with histologic pattern and direction of spread. *Am J Surg Pathol.* 1988; 12:897–906. DOI: 10.1097/00000478-198812000-00001 [PubMed: 3202246]
4. Augustin H, Erbersdobler A, Graefen M, Fernandez S, Palisaar J, Huland H, et al. Biochemical recurrence following radical prostatectomy: A comparison between prostate cancers located in different anatomical zones. *Prostate.* 2003; 55:48–54. DOI: 10.1002/pros.10216 [PubMed: 12640660]
5. Carroll PR, Parsons JK, Andriole G, Bahnson RR, Barocas Da, Catalona WJ, et al. Prostate Cancer Early Detection, Version 1.2014: Featured Updates to the NCCN Guidelines. *J Natl Compr Cancer Netw.* 2014; 12:1211–9.
6. Johnson LM, Turkbey B, Figg WD, Choyke PL. Multiparametric MRI in prostate cancer management. *Nat Rev Clin Oncol.* 2014; 11:346–53. DOI: 10.1038/nrclinonc.2014.69 [PubMed: 24840072]
7. Wu LM, Xu JR, Ye YQ, Lu Q, Hu JN. The clinical value of diffusion-weighted imaging in combination with T2-weighted imaging in diagnosing prostate carcinoma: A systematic review and meta-analysis. *Am J Roentgenol.* 2012; 199:103–10. DOI: 10.2214/AJR.11.7634 [PubMed: 22733900]
8. Isebaert S, Van Den Bergh L, Haustermans K, Joniau S, Lerut E, De Wever L, et al. Multiparametric MRI for prostate cancer localization in correlation to whole-mount histopathology. *J Magn Reson Imaging.* 2013; 37:1392–401. DOI: 10.1002/jmri.23938 [PubMed: 23172614]
9. Rosenkrantz AB, Taneja SS. Radiologist, be aware: Ten pitfalls that confound the interpretation of multiparametric prostate MRI. *Am J Roentgenol.* 2014; 202:109–20. DOI: 10.2214/AJR.13.10699 [PubMed: 24370135]
10. White NS, Leergaard TB, D'Arceuil H, Bjaalie JG, Dale AM. Probing tissue microstructure with restriction spectrum imaging: Histological and theoretical validation. *Hum Brain Mapp.* 2013; 34:327–46. DOI: 10.1002/hbm.21454 [PubMed: 23169482]
11. Farid N, Almeida-Freitas DB, White NS, McDonald CR, Kuperman JM, Almutairi Aa, et al. Combining diffusion and perfusion differentiates tumor from bevacizumab-related imaging abnormality (bria). *J Neurooncol.* 2014; 120:539–46. DOI: 10.1007/s11060-014-1583-2 [PubMed: 25135423]
12. White NS, McDonald CR, Farid N, Kuperman J, Karow D, Schenker-Ahmed NM, et al. Diffusion-Weighted Imaging in Cancer: Physical Foundations and Applications of Restriction Spectrum Imaging. *Cancer Res.* 2014; 74:4638–52. DOI: 10.1158/0008-5472.CAN-13-3534 [PubMed: 25183788]
13. Liss MA, White NS, Parsons JK, Schenker-Ahmed NM, Rakow-Penner R, Kuperman JM, et al. MRI-Derived Restriction Spectrum Imaging Cellularity Index is Associated with High Grade Prostate Cancer on Radical Prostatectomy Specimens. *Front Oncol.* 2015; 5:1–8. DOI: 10.3389/fonc.2015.00030 [PubMed: 25667919]
14. Rakow-Penner RA, White NS, Parsons JK, Choi HW, Liss Ma, Kuperman JM, et al. Novel technique for characterizing prostate cancer utilizing MRI restriction spectrum imaging: proof of principle and initial clinical experience with extraprostatic extension. *Prostate Cancer Prostatic Dis.* 2015; 18:81–5. DOI: 10.1038/pcan.2014.50 [PubMed: 25559097]
15. Holland D, Kuperman JM, Dale AM. Efficient correction of inhomogeneous static magnetic field-induced distortion in Echo Planar Imaging. *Neuroimage.* 2010; 50:175–83. DOI: 10.1016/j.neuroimage.2009.11.044 [PubMed: 19944768]
16. Epstein JI, Allsbrook WCJ, Amin MB, Egevad LL. The 2005 International Society of Urological Pathology (ISUP) Consensus Conference on Gleason Grading of Prostatic Carcinoma. *Am J Surg Pathol.* 2005; 29:1228–42. DOI: 10.1097/01.pas.0000173646.99337.b1 [PubMed: 16096414]
17. Epstein JI, Zelefsky MJ, Sjoberg DD, Nelson JB, Egevad L, Magi-Galluzzi C, et al. A Contemporary Prostate Cancer Grading System: A Validated Alternative to the Gleason Score. *Eur Urol.* 2015; :1–8. DOI: 10.1016/j.eururo.2015.06.046
18. Gleason DF. Classification of prostatic carcinomas. *Cancer Chemother Reports.* 1966; 50:125–8.

19. Bates D, Mächler M, Bolker BM, Walker SC. Fitting linear mixed-effects models using lme4. *J Stat Softw.* 2015; 67:1–48.
20. Hothorn T, Bretz F, Westfall P. Simultaneous inference in general parametric models. *Biometrical J.* 2008; 50:346–63. DOI: 10.1002/bimj.200810425
21. R Core Team. *R: A language and environment for statistical computing.* Vienna, Austria: R Foundation for Statistical Computing; 2015.
22. McCammack KC, Kane CJ, Parsons JK, White NS, Schenker-Ahmed NM, Kuperman JM, et al. In vivo prostate cancer detection and grading using Restriction Spectrum Imaging-MRI. *Prostate Cancer Prostatic Dis.* 2016 Jan 12. [Epub ahead of print].
23. Hricak H, Dooks GC, McNeal JE, Mark aS, Marotti M, Avallone a, et al. MR imaging of the prostate gland: normal anatomy. *AJR Am J Roentgenol.* 1987; 148:51–8. DOI: 10.2214/ajr.148.1.51 [PubMed: 3491523]
24. Myers RP. Structure of the Adult Prostate From a Clinician's Standpoint. *Clin Anat.* 2000; 215:214–5. [PubMed: 10797630]

Translational Relevance: Current multiparametric magnetic resonance imaging (MP-MRI) techniques for detecting prostate cancer are limited with respect to tumor conspicuity assessment, in vivo characterization and localization. We have demonstrated that a novel diffusion-based MRI technique, restriction spectrum imaging (RSI-MRI), differentiates among benign, low-grade and high-grade PCa at a voxel-level resolution. Use of an RSI-MRI index to differentiate between clinically relevant low- and high-grade categories of tumor PCa aggressiveness may help improve and refine diagnosis and staging of PCa. Additionally, because it can detect intratumor variation, RSI-MRI may have particular relevance for the planning targeted therapies such as radiation seed therapy placement, magnetic resonance (MR)-guided focused ultrasound surgery, and MR-guided targeted biopsy.

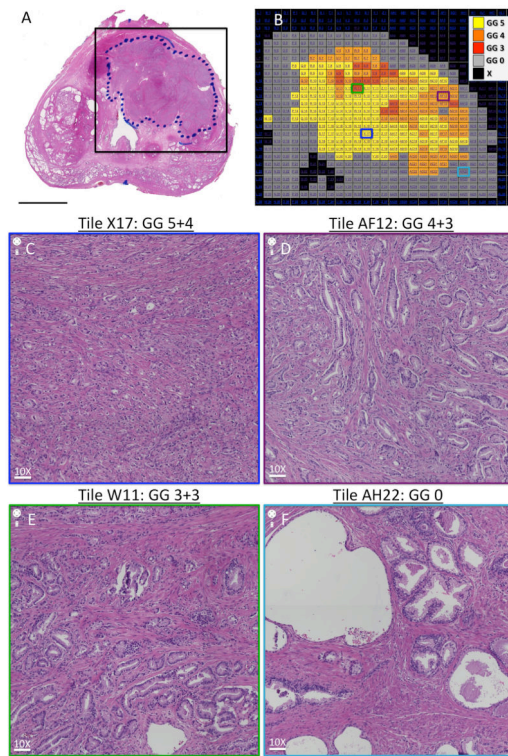


Fig. 1. “Digital prostate map” histopathological section and example grid overlay
 (A) H&E-stained WM histopathological prostate with a black box surrounding tumor ROI that represents the boundaries of a grid for sectioning the tumor area into voxel-sized tiles for grading purposes. Scale bar = 1 cm. (B) H&E-stained WM histopathological prostate section reconstructed into a “digital prostate map” interface online. Alphanumeric grid represents the outlined box in (A) surrounding the tumor ROI. Gleason grade is coded by color as defined by the key. (C) Representative tile (X17), showing Gleason grade 5+4 = 9 tumor architecture at 10X magnification. Scale bar = 75.5 μ m. (D) Representative tile (AF12), showing Gleason grade 4+3 = 7 tumor architecture at 10X magnification. Scale bar = 75.5 μ m. (E) Representative tile (W11), showing Gleason grade 3+3 = 6 tumor architecture at 10X magnification. Scale bar = 75.5 μ m. (F) Representative tile (AH22), showing benign architecture at 10X magnification. Scale bar = 75.5 μ m. Abbreviations: GG, Gleason grade; H&E, haematoxylin & eosin; ROI, region of interest; WM, whole mount.

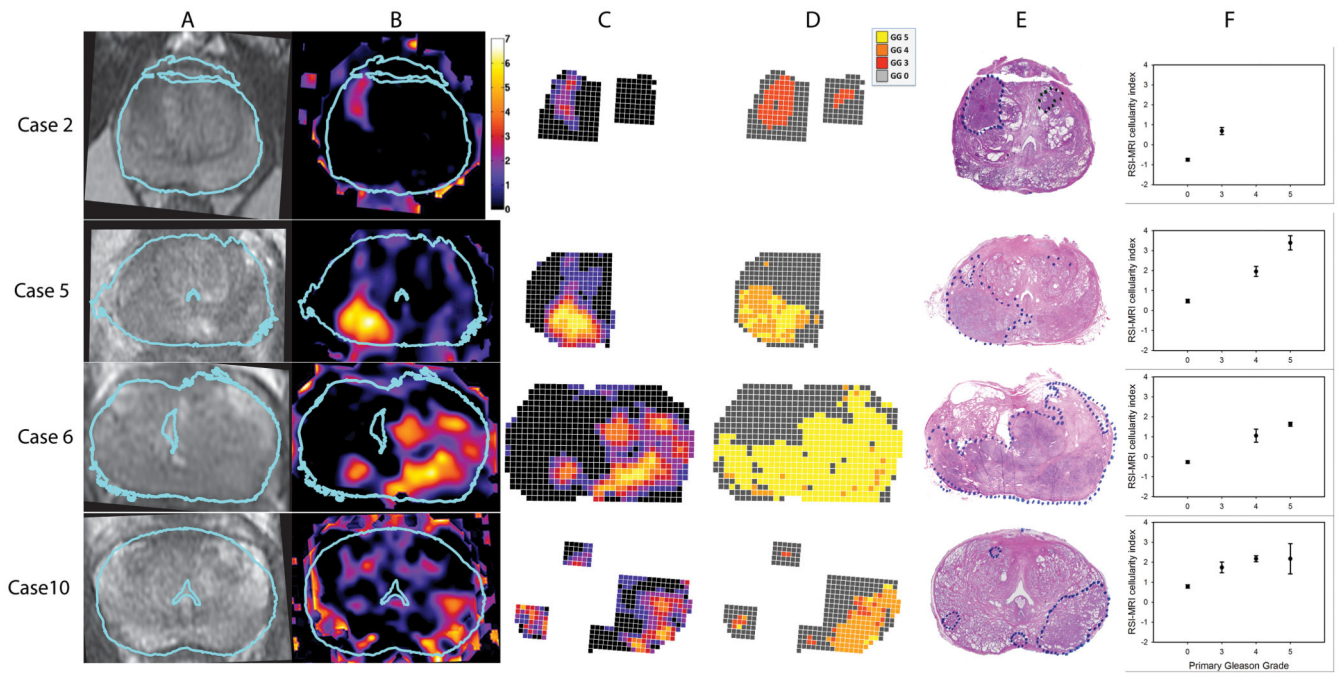


Fig. 2. T2, RSI-MRI, Gleason grade, and H&E: Cases 2, 5, 6, and 10

A) T2-weighted MR images, after in-plane affine transformation to correspond to the histopathology slides, B) RSI-MRI color coded cellularity maps, C) “Digital prostate map” grid overlay color-coded for RSI-MRI cellularity index, D) “Digital prostate map” grid overlay color-coded for Gleason grade, E) H&E-stained WM histopathological prostate section with tumor area(s) outlined, F) Plots for each case of the mean RSI-MRI signal corresponding to each histological Gleason grade based on voxel-level analysis. Error bars represent the standard errors of the mean. Blue outline in A&B indicates the correspondence of the histopathology slide to the MR image. Abbreviations: H&E, haematoxylin & eosin; MR, magnetic resonance; RSI, restriction spectrum imaging; WM, whole mount.

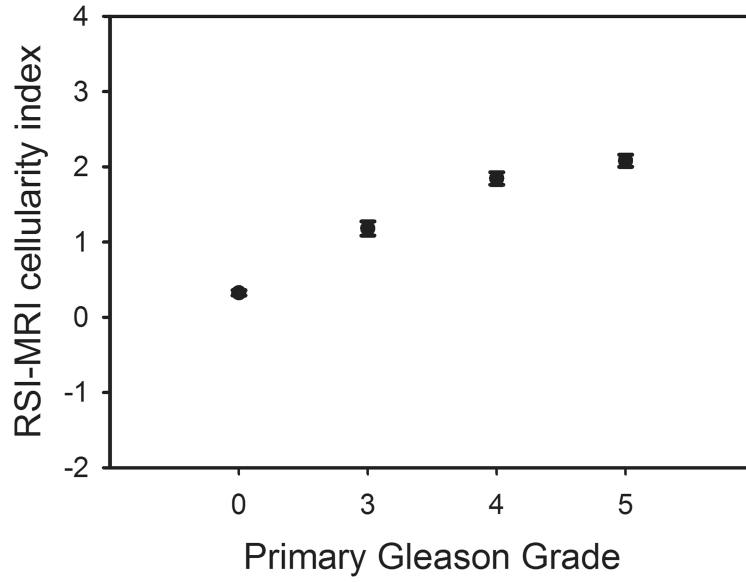


Fig. 3. RSI-MRI mean cellularity index grouped by pathologic Gleason grade
Mean RSI-MRI cellularity index represented as a z-score corresponding to histological Gleason grade using data from all voxels graded in all cases. Error bars represent the standard errors of the mean.

Author Manuscript

Author Manuscript

Author Manuscript

Author Manuscript

Table 1
Demographics of ten patients who had a pre-operative MRI with subsequent radical prostatectomy.

Case	Race	Age	PSA	Clinical Stage	Location of Positive Biopsy ^a	Biopsy Grade	Days between Biopsy and MRI	Positive Cores	Tumor Volume (%)	WM Grade	Pathologic Stage
1	White	61	9.8	T1c	L. Lateral Base L. Medial Base	3+4 3+3	553	2 of 12	1.3	3+4 ^b	pT2cNX
2	White	58	5.7	T2a	R. Mid L. Lateral Base L. Apex	3+4 3+4 3+4	314	3 of 12	9	3+3 ^b	pT2cN0
3	White	68	4.7	T1c	L. Lateral Base L. Lateral Mid	3+4 3+4	65	2 of 12	2.9	4+3	pT2aN0
4	White	73	6.2	T1c	L. Apex L. Lateral Mid R. Lateral Mid	3+4 3+3 3+3	97	3 of 19	12.6	5+3	pT2cN0
5	White	69	7.4	T2c	R. Lateral Apex ^c R. Lateral Mid ^c R. Lateral Base ^c R. Medial Base ^c L. Lateral Mid ^f L. Lateral Base L. Medial Mid ^f	5+4 3+5 5+4 5+5	33	7 of 12	18 0.8 0.28	4+5 ^d 4+5 ^e 3+3 ^e	pT3aN0
6	White	54	16.7	T2c	R. Lateral Base R. Medial Base R. Medial Mid L. Lateral Apex L. Lateral Mid L. Lateral Base L. Medial Mid ^f	4+5 5+5 5+5 5+4 5+4 5+4 5+5	26	9 of 14	60-70	5+4	pT3bN1
7	White	68	21.5	T1c	R. Medial Apex ^g	4+3	33	5 of 17	26	4+4	pT3aN0
8	White	66	1.05	T2a	R. Lateral Mid	3+3	61	1 of 12	5.3 1	3+4 3+3 ^b	pT2cNX
9	White	63	9.4	T1c	Not specified	3+3	127	2 of 7	<2	4+3 ⁱ	pT2cNX
10	African American	51	9.3	T1c	L. Lateral Mid >L. Lateral Apex	3+4 3+4	85	2 of 14	4.4 <1	4+3 ^j 3+3 ^k	pT2cN0

^aStandard 12-core biopsies.

^badditional outlined tumors of concurrent grade marked by pathologist.

Author Manuscript

Author Manuscript

Author Manuscript

Author Manuscript

- ^cintraductal carcinoma,
- ^ddominant tumor in R. apex to base,
- ^eadditional tumors in L. Base and L. Apex,
- ^fhigh grade prostatic intraepithelial neoplasia,
- ^gFive out of six cores for the R. Medial Apex were contained adenocarcinoma,
- ^hScattered microscopic foci,
- ⁱTwo additional microscopic foci present,
- ^jDominant tumor in L. mid lateral with additional outlined tumors of concurrent grade in the R. mid prostate, R. apex, and L. base,
- ^kMultiple microscopic foci.
- Abbreviations: L., Left; Med., Medial; MRI, magnetic resonance imaging; PSA, prostate serum antigen; R., Right; WM, whole mount.

Table 2

Voxel level statistical analysis of RSI-MRI cellularity index versus benign or malignant tissue in histopathological section (Gleason grades 3-5). A linear mixed-effects model with a random effect of subject was implemented to compare difference in detection among benign tissue vs. low grade PCa (primary Gleason 3) vs. high grade PCa (primary Gleason 4).

Random effects: Subject					
	(Intercept)	Residual			
Std. Dev	0.7444	1.423			

Fixed effects: RSI-MRI cellularity index vs. PCa tumor grade					
	Value	Std. Error	DF	t-value	p-value
(Intercept)	0.1589	0.2386	2783	0.6660	0.5055
Low-grade	1.153	0.0998	2783	11.56	$<1 \times 10^{-5}$
High-grade	1.516	0.0631	2783	24.03	$<1 \times 10^{-5}$

Abbreviations: PCa, prostate cancer; DF, degrees of freedom

Table 3

Voxel level statistical comparing RSI-MRI cellularity index between prostate cancer Gleason categories versus normal tissues and between pathological grades. Post-hoc multiple comparison *t*-tests were implemented in comparing difference in detection of PCa aggressiveness (low grade PCa (primary Gleason 3) and high grade PCa (primary Gleason 4)) vs. benign tissue and between tumor grades (low grade PCa vs. high grade PCa).

Group	Mean difference (standard error)	<i>p</i> -value
Pathology vs. normal		
Low grade vs. normal	1.153 (0.100)	< 0.001
High grade vs. normal	1.516 (0.063)	< 0.001
Between Pathological grades		
High grade vs. Low Grade	0.364 (0.113)	= 0.003

Abbreviations: PCa, prostate cancer

Author Manuscript

Author Manuscript

Author Manuscript

Author Manuscript